JOURNAL OF COMPUTATIONAL PHYSICS 104, 329–346 (1993)

Characteristic Multigrid Method Application to Solve the Euler Equations with Unstructured and Unnested Grids

M. P. LECLERCQ AND B. STOUFFLET

Dassault Aviation, 78 quai Marcel, Dassault, 92214 Saint-Cloud, France

Received March 28, 1991; revised February 18, 1992

A new multigrid method for the solution of hyperbolic systems of conservation laws (such as the Euler equations of compressible inviscid flows), combined with higher-order upwind approximation, is constructed. The novelty of the method lies in the introduction of an upwind transfer operator between two successive grids. First, the efficiency of the method is investigated for a scalar linear advection equation in one dimension of space using Fourier analysis. An extension to an unstructured multigrid method is then proposed. Numerical results for two-dimensional flow computations including hypersonic flow simulation are presented. © 1993 Academic Press, Inc.

1. INTRODUCTION

The general multigrid algorithm has now proved to be one of the most efficient methods of accelerating the convergence of a numerical scheme to the steady-state solution of a system of non-linear equations. The basic idea is to compute approximate corrections obtained on coarser meshes and transfer them to the fine grid solution. These corrections, derived from the problem equations, do not affect the accuracy of the fine grid solution but significantly increase the rate of convergence of the basic numerical scheme. This method was first applied to solving elliptic problems where the theory is now well established [8, 20]. Although theoretical results remain very poor for hyperbolic problems, successful applications of the multigrid method have been performed. Among others, Ni [23] and Jameson [10] have developed two reference multigrid methods to solve the Euler equations in the framework of structured meshes.

Today, the use of unstructured meshes is widespread [11, 19, 25, 9, 30] in the CFD community to solve the steady-state Euler equations. These methods are now competitive compared to the available structured-mesh solvers and efficient vectorization can be achieved with coloured graph algorithms [29] on supercomputers. The efficiency of the method has been demonstrated when combined with structured meshes; therefore the need to develop such algorithms in the unstructured context has emerged.

The multigrid method used with the structured-mesh solvers relies on nested meshes; this property can no longer be preserved in our context because the quality of the finest grid will heavily depend on the definition of the coarse level even if subdivisions of the elements are performed only in selected regions of the domain (combined with adaptive mesh enrichment) [26]. One must design a more general non-linear multigrid algorithm. Such an algorithm operating on a sequence of completely unrelated unstructured coarse and fine meshes has been described in [21] in the two-dimensional case. It relies on a centered finite-volume discretization of the Euler equations with added artificial dissipation, the integration in time being carried out by a fully explicit five-stage time-stepping scheme. Grid transfer operators use the shape functions associated with a piecewise linear approximation in each element.

An alternate approach is to generate coarse levels from an arbitrary unstructured triangulation, taking advantage of the finite volume discretization on a dual mesh partitioned in control volumes. This procedure has been successfully applied [14], combined with the explicit second-order accurate upwind nodal approximation described in [7].

Recently, Leclercq *et al.* [15] developed a multigrid method called the GM (geometric multigrid) method by retaining the approach of Mavriplis and Jameson [21], which uses a sequence of completely unrelated unstructured meshes, and by extending this idea to the aforementioned second-order accurate upwind approximation, in two and three dimensions.

The methods mentioned above have proved to be very efficient in solving transonic and supersonic problems, but show a lack of robustness when dealing with high Mach number flow simulations. Furthermore, when using the GM method in some situations, the residual enters a limit cycle of oscillations probably due to the inability of the method to damp the high frequencies of the error in a satisfactory way. It is believed that one of the reasons for these failures lies in

0021-9991/93 $5.00

the fact that transfer operators, from one grid to another, are purely interpolation operators designed for elliptic problems and do not take the hyperbolicity of the Euler equations into account. This aspect was first investigated by Sanders [27] and some developments in this direction have been performed by Koren [12].

This paper discusses an attempt to design better adapted transfer operators in a multigrid algorithm in order to solve hyperbolic problems. Thus, we will particularly analyze some *upwind* transfer operators.

First, we present in Section 2 the multigrid algorithm with general transfer operators. Then in Section 3, the sensitivity of the transfer operator upwinding for accelerating an explicit multistage iterative solver is studied on a one-dimensional linear advection equation through a Fourier analysis. This study will demonstrate the superiority of introducing upwinding. In Section 4, the adaptation of this technique to the two-dimensional GM method is proposed in the unstructured mesh context. Finally, two-dimensional results with the new CM (characteristic multigrid) method will be presented to illustrate the extended capacities of the multigrid algorithm.

2. MULTIGRID ALGORITHM—GENERAL CASE

The purpose of this section is to describe, in a general pattern, the non-linear multigrid method FAS (full approximation scheme) [2, 3, 8], and to introduce the notations and key words that will be used through out this paper. The description is restricted to the case of two computational grids. We consider a general non-linear steady-state problem in a domain $\Omega \subset \mathbb{R}^d$, with boundary Γ:

$$\begin{aligned} &F(w(x)) = S, \qquad x \in \Omega \\ &\quad + \text{boundary conditions on } \Gamma \end{aligned} \tag{1}$$

where $w: \mathbb{R}^d \to \mathbb{R}^n$ and $F: \mathbb{R}^n \to \mathbb{R}^m$.

It is well known that the solution of problem (1) can be considered as an asymptotic particular solution of the following time-dependent problem:

$$\begin{aligned} &\frac{\partial}{\partial t} w(x,t) + F(w(x,t)) = S, \qquad t \in \mathbb{R}^+, \quad x \in \Omega \\ &\quad + \text{boundary conditions on } \Gamma \\ &w(x,0) = w^0(x), \qquad x \in \Omega \quad \text{(initial data)}. \end{aligned} \tag{2}$$

In the framework of multigrid method, we assume that X_h, Y_h, X_H, and Y_H ($\Delta x_H > \Delta x_h$) are the functional discretization spaces for w_h, $F_h(w_h)$, w_H, and $F_H(w_H)$, respectively. After discretization, problem (2) becomes

$$\begin{aligned} &\frac{\partial}{\partial t} w_h(t) + F_h(w_h(t)) = S_h, \qquad t \in \mathbb{R}^+ \\ &\quad + \text{boundary conditions on } \Gamma \\ &w_h(0) = w_h^0 \quad \text{(initial data)}. \end{aligned} \tag{3}$$

The scheme used to solve (3) is called the *basic scheme on grid* G_h and denoted by $BS_h: X_h \to Y_h$.

We should define the three transfer operators $\mathbf{I}_{h \mapsto H}$, $\bar{\mathbf{I}}_{h \mapsto H}$, and $\mathbf{I}_{H \mapsto h}$ which are needed for the restriction of variable w_h, the restriction of residual $(F_h(w_h) - S_h)$, and the prolongation of coarse grid correction C_H, respectively. These definitions are summarized in Fig. 1.

TWO-GRID ALGORITHM. Let $w_h^n = w_h(t^n) \in X_h$ be the solution of (3) at the time t^n. Hereafter we describe one cycle of the multigrid algorithm which computed the new iterate w_h^{n+1} from w_h^n.

1. An approximate solution $w_h^a \in X_h$ is computed by applying ν_h^1 iterations of the basic scheme BS_h:

$$\begin{aligned} &\bar{w}_h^0 = w_h^n, \\ &\bar{w}_h^\nu = BS_h(\bar{w}_h^{\nu-1}), \qquad \nu = 1, \ldots, \nu_h^1, \\ &w_h^a = \bar{w}_h^{\nu_h^1}, \end{aligned}$$

2. The problem on the coarse grid can be written in a form similar to that of (3) on the fine grid:

$$\begin{aligned} &\frac{\partial}{\partial t} w_H + F_H(w_H) = S_H \qquad \text{in the domain } \Omega \\ &\quad + \text{boundary conditions on } \Gamma \\ &w_H(0) = w_H^0 = \mathbf{I}_{h \mapsto H}(w_h^a) \qquad \text{(initial data)}, \end{aligned} \tag{4}$$

where the source term S_H is defined as

$$S_H = F_H(w_H^0) - \bar{\mathbf{I}}_{h \mapsto H}(F_h(w_h^a) - S_h).$$

Let $BS_H: X_H \to Y_H$ denote the basic scheme associated with problem (4).

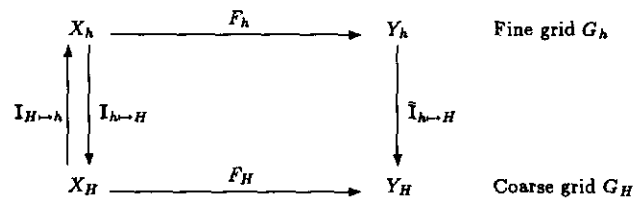

FIG. 1. General transfer operators.

3. After applying v_H^1 iterations of the basic scheme BS_H, we get an approximate solution $w_H^* \in X_H$ to problem (4):

$$w_H^v = BS_H(w_H^{v-1}), \qquad v = 1, ..., v_H^1,$$
$$w_H^* = w_H^{v_H^1}.$$

4. The coarse grid correction is then defined as

$$C_H = w_H^* - w_H^0 = w_H^* - \mathbf{I}_{h \mapsto H}(w_h^a).$$

5. Finally, the coarse grid correction is interpolated on the fine level and added to the approximate solution $w_h^a \in X_h$ to obtain the corrected solution $w_h^c \in X_h$,

$$w_h^c = w_h^a + \mathbf{I}_{H \mapsto h}(C_H)$$

Before updating the solution $w_h^{n+1} \in x_h$, v_h^2 iterations of the basic scheme, acting on X_h, are performed:

$$\bar{w}_h^0 = w_h^c$$
$$\bar{w}_h^v = BS_h(\bar{w}_h^{v-1}), \qquad v = 1, ..., v_h^2,$$
$$w_h^{n+1} = \bar{w}_h^{v_h^2}$$

Remark 1. The parameter v_h^2 plays an important role when the number of computational grids is greater than two. The effect of this parameter on the global efficiency of the method will not be studied in this paper (in practice, we will take $v_h^2 = 0$).

Remark 2. Extending the above two-grid algorithm to the multigrid case is straightforward using induction on the number of grids.

FULL-MULTIGRID ALGORITHM. The full-multigrid method is a combination of the multigrid algorithm described previously and the successive refinement technique. In case of N computational grids, from the coarsest one G_1 to the finest one G_N, the algorithm can be written as follows:

1. Single-grid solution on grid G_1. From the initial solution w_1^i, an approached solution (final solution) w_1^f is obtained by applying the single grid scheme.

2. For $l = 2$ to N the following process is performed: From the initial solution on level l, defined as the interpolation of the final solution on level $l-1$, i.e., $w_l^i = \mathbf{I}_{H \mapsto h}(w_{l-1}^f)$; the final solution on level l, w_l^f is obtained by applying the l-grid scheme.

The final solution of the algorithm is thus w_N^f, with the above notations.

3. ONE-DIMENSIONAL CASE–FOURIER ANALYSIS

The damping of the high frequencies or the highest frequency of the error is a necessary property of the basic scheme to be used as a smoother of a multigrid method. The purpose of this section is to examine the damping properties of a four-stage scheme which is associated with an upwind second-order accurate space approximation in order to solve hyperbolic problems. The resulting basic scheme will be used later to solve the steady-state Euler equations with a pseudo-unsteady multigrid method in a finite element context. The model problem is the scalar linear advection equation, which is usually considered to analyze the stability and the precision of hyperbolic solvers [32]. We will obtain the scheme amplification factor by Fourier analysis, i.e., by the Fourier transform of the basic scheme operator. We will compare results obtained when considering the single-grid scheme amplification factor only, with results given by a genuine analysis of the amplification factor of an ideal two-grid cycle (convergence on the coarse grid is then supposed to be complete). The analysis of the single-grid amplification factor is performed in order to select the optimal (in some sense) multi-stage scheme of the multigrid method. Two criteria are considered; optimization is made with respect to the damping of higher frequencies [10, 18, 31] and to the highest frequency [13].

On the other hand, the study of the amplification factor of the ideal two-grid cycle allows the direct optimization of the coefficients of the multi-stage scheme. Furthermore, this optimization takes into account the transfer operators and gives an optimal multi-stage scheme for any multigrid method. This study can be related to the work of V. Couailler *et al.* [4, 5] for a two-grid V-cycle of a predictor–corrector Lax–Wendroff scheme, of Jameson [10] and of Mulder [22]. We will then try to improve the two-grid scheme (through its amplification factor) by modifying the transfer operators definition.

3.1. *Model Problem*

We consider the scalar linear advection equation (with $c \in \mathbb{R}^*$) in the interval $\Omega \subset \mathbb{R}$ with boundary Γ:

$$\frac{\partial}{\partial t} w(x, t) + c \frac{\partial}{\partial x} w(x, t) = 0, \quad x \in \mathbb{R}, \quad t \in \mathbb{R}^+$$
$$+ \text{boundary conditions on } \Gamma \tag{5}$$
$$w(x, 0) = w^0(x) \quad \text{(initial data)}.$$

Remark 3. Problem (5) is equivalent to problem (2) with:

$$F(w(x, t)) = c \frac{\partial}{\partial x} w(x, t), \qquad S = 0, \quad \Omega \subset \mathbb{R}.$$

We assume that $w(x, t)$ is periodic, with a period equal to one, so the discretization domain is reduced to the interval $[0, 1]$.

To discretize problem (5), spatial upwind approximation and time integration should now be specified. Let G_g be a standard discretization of $[0, 1]$ with space-step $\Delta x_g = 1/n_g$, $n_g \in \mathbb{N}^*$; we denote by $x_j = j\,\Delta x_g$ the nodes and by $C_{g_j} =]x_{j-1/2}, x_{j+1/2}[$ the cells (with $x_{j\pm 1/2} = x_j \pm \Delta x_g/2$), for $j = 0, ..., n_g$.

We denote by $c^+ = \max(c, 0)$ and $c^- = \min(c, 0)$ ($c = c^+ + c^-$). Use upwind differencing for the spatial derivative, and integrate Eq. (5) on C_{g_j} (for $j = 0, ..., n_g$); then obtain the semi-discrete scheme,

$$\begin{aligned} &\frac{\partial}{\partial t} w_{g_j}(t) = -\frac{1}{\Delta x_g} R_{g_j} \\ &\qquad w_{g0} = w_{g_{n_g}} \qquad \text{(periodicity)} \\ &w_{g_j}(0) = w_j^0 \qquad \text{(initial data)}, \end{aligned} \tag{6}$$

where $w_{g_j}(t)$ denotes $w(x_j, t)$ and the residual R_{g_j} is defined as:

$$\begin{aligned} R_{g_j} \overset{\text{def}}{=} c^+ &[w^-_{g_{j+1/2}}(t) - w^-_{g_{j-1/2}}(t)] \\ &+ c^- [w^+_{g_{j+1/2}}(t) - w^+_{g_{j-1/2}}(t)]. \end{aligned} \tag{7}$$

The solution $w_g(t)$ is a priori, not continuous at nodes $x_{j\pm 1/2}$ but its limits are known:

$$\begin{aligned} w^-_{g_{j\pm 1/2}}(t) &= \lim_{\substack{x < x_{j\pm 1/2} \\ x \to x_{j\pm 1/2}}} w(x, t); \\ w^+_{g_{j\pm 1/2}}(t) &= \lim_{\substack{x > x_{j\pm 1/2} \\ x \to x_{j\pm 1/2}}} w(x, t). \end{aligned} \tag{8}$$

For first-order space accuracy, $w_g(t)$ is taken as a constant on the cell C_{g_j}; the limits in (8) are then given by

$$\begin{aligned} w^-_{g_{j+1/2}}(t) &= w_{g_j}(t) \\ w^+_{g_{j+1/2}}(t) &= w_{g_{j+1}}(t). \end{aligned} \tag{9}$$

For higher-order space accuracy, a MUSCL approach [16] is considered ($w_g(t)$ is taken as piecewise linear on each cell C_{g_j}); the limits in (8) are then given by the formulae

$$\begin{aligned} w^-_{g_{j+1/2}}(t) = w_{g_j}(t) &+ \frac{1-\kappa}{4} [w_{g_j}(t) - w_{g_{j-1}}(t)] \\ &+ \frac{1+\kappa}{4} [w_{g_{j+1}}(t) - w_{g_j}(t)] \end{aligned}$$

$$\begin{aligned} w^+_{g_{j+1/2}}(t) = w_{g_{j+1}}(t) &- \frac{1-\kappa}{4} [w_{g_{j+2}}(t) - w_{g_{j+1}}(t)] \\ &- \frac{1+\kappa}{4} [w_{g_{j+1}}(t) - w_{g_j}(t)], \end{aligned} \tag{10}$$

where the parameter $\kappa \in [-1, 1]$ can be chosen to select the level of the interpolation ($\kappa = 1$ corresponds to a central differencing, $\kappa = -1$ corresponds to a second-order accurate fully upwind differencing, $\kappa = 0$ corresponds to a second-order accurate half-upwind (Fromm) differencing, $\kappa = \frac{1}{3}$ corresponds to a third-order accurate upwind differencing [6, 17]).

The time integration is performed with a four-stage time-stepping scheme. The solution $w_g^{n+1} = (w_{g_j}(t^{n+1}))_{j=1,...,n_g}$ is obtained from the solution $w_g^n = (w_{g_j}(t^n))_{j=1,...,n_g}$ with the iterative process,

$$\begin{aligned} &\bar{w}_g^{(0)} \overset{\text{def}}{=} w_g^n \\ &\bar{w}_g^{(k)} = \bar{w}_g^{(0)} - \alpha_{g_k} \frac{\Delta t_g}{\Delta x_g} R_g(\bar{w}_g^{(k-1)}), \quad k = 1, ..., 4 \\ &w_g^{n+1} \overset{\text{def}}{=} \bar{w}_g^{(4)}, \end{aligned} \tag{11}$$

where $\alpha_{g_k} \in [0, 1]$ for $k = 1, ..., 3$ and $\alpha_{g_4} = 1$ are the time-stepping scheme coefficients associated with the approximation on the grid G_g. Process (11) constitutes the basic scheme of the multigrid method.

3.2. *Fourier Analysis*

We are interested in analyzing the behavior of the multigrid method amplification factor with a four-stage time-stepping as a basic scheme. Let us carry out a study based on a Fourier analysis and insert harmonic data:

$$\begin{aligned} &w_{g_j}^n = \hat{w}_g^n e^{ij\theta_g}, \qquad j = 1, ..., n_g \\ &\theta_g = -2\pi k\,\Delta x_g, \qquad k = 1, ..., n_g - 1. \end{aligned}$$

The residual of Eq. (7) becomes $\hat{R}_g = (|c|\, z_g(\theta_g)\, \hat{w}_g)$, where $z_g(\theta_g) \in \mathbb{C}$ results from relations (12) (obtained from (9)) and (13) (obtained from (10)) for first order and higher order spatial accuracy, respectively,

First order:

$$z_g(\theta_g) = \frac{c^+}{|c|} [1 - e^{-i\theta_g}] + \frac{c^-}{|c|} [e^{i\theta_g} - 1] \tag{12}$$

Higher order:

$$z_g(\theta_g) = \frac{c^+}{|c|}(1 - e^{-i\theta_g}) \times \left(1 + \frac{1-\kappa}{4}(1 - e^{-i\theta_g}) + \frac{1+\kappa}{4}(e^{i\theta_g} - 1)\right) + \frac{c^-}{|c|}(e^{i\theta_g} - 1) \times \left(1 - \frac{1-\kappa}{4}(e^{i\theta_g} - 1) - \frac{1+\kappa}{4}(1 - e^{-i\theta_g})\right). \quad (13)$$

The iterated solution $\hat{w}_g^{n+1}$ is then given by the scalar equation

$$\hat{w}_g^{n+1} = g_g(\alpha_g, \sigma_g, \theta_g)\, \hat{w}_g^n,$$

where $g_g(\alpha_g, \sigma_g, \theta_g)$ is the Fourier transform of the basic scheme operator BS_g and can be written as a polynomial of $z_g(\theta_g)$,

$$g_g(\alpha_g, \sigma_g, \theta_g) = 1 - \sigma_g z_g(\theta_g) + \alpha_{g_3}\sigma_g^2 z_g^2(\theta_g) - \alpha_{g_2}\alpha_{g_3}\sigma_g^3 z_g^3(\theta_g) + \alpha_{g_1}\alpha_{g_2}\alpha_{g_3}\sigma_g^4 z_g^4(\theta_g), \quad (14)$$

where $\sigma_g = |c|(\Delta t_g/\Delta x_g)$ denotes the Courant–Friedrichs–Lewy (CFL) number.

The single-grid amplification factor $\mathscr{AF}_g(\alpha_g, \sigma_g, \theta_g)$ is then defined as the modulus of the complex term $g_g(\alpha_g, \sigma_g, \theta_g)$.

To estimate the amplification factor of one multigrid cycle, we have to extend the previous analysis to all steps of the multigrid algorithm. To make it clearer, we will consider in the following the two-grid method relying on a fine grid G_h ($\Delta x_h = 1/n_h$, $n_h \in \mathbb{N}^*$, n_h an even number) and a coarse one G_H ($\Delta x_H = 2\Delta x_h$), deduced from G_h by eliminating odd-numbered nodes (grids G_h and G_H are nested). We then define transfer operators in a general form:

• $\mathbf{I}_{h \mapsto H}$, used for the restriction of w_h. We consider the simplest restriction:

$$\mathbf{I}_{h \mapsto H}(w_h)_{2p} = w_{h_{2p}} \quad \text{for} \quad p = 0, ..., n_h/2. \quad (15)$$

• $\bar{\mathbf{I}}_{h \mapsto H}$, used for the restriction of residuals R_h. This operator has to be conservative. The residual at coarse node

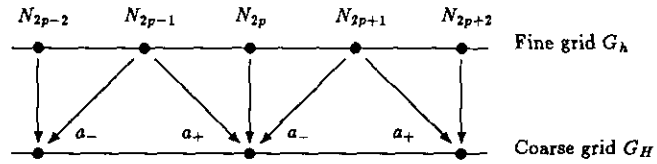

FIG. 2. Operator $\bar{\mathbf{I}}_{h \mapsto H}$ in 1D.

N_{2p} is a weight-average of the residuals at fine nodes N_{2p-1}, N_{2p}, and N_{2p+1}:

$$\bar{\mathbf{I}}_{h \mapsto H}(R_h)_{2p} = a_+ R_{h2p-1} + R_{h2p} + a_- R_{h2p+1} \quad \text{for} \quad p = 0, ..., n_h/2, \quad (16)$$

where the coefficients a_+ and a_- ($\in [0, 1]$) are interpolation weights such that $a_+ + a_- = 1$ to ensure the conservation. This transfer is sketched in Fig. 2.

• $\mathbf{I}_{H \mapsto h}$, used for the prolongation of corrections (C_H). The interpolation operates differently for odd-numbered and even-numbered nodes,

$$\mathbf{I}_{H \mapsto h}(C_H)_{2p} = (C_H)_{2p} \quad \text{for} \quad p = 0, ..., n_h/2$$
$$\mathbf{I}_{H \mapsto h}(C_H)_{2p+1} = b_+ C_{H_{2p}} + b_- C_{H_{2p+2}} \quad \text{for} \quad p = 0, ..., (n_h - 1)/2, \quad (17)$$

where the coefficients b_+ and b_- ($\in [0, 1]$) are interpolation weights such that $b_+ + b_- = 1$. This transfer is sketched in Fig. 3.

As it appears in the definition of the transfer operator $\mathbf{I}_{H \mapsto h}$ (17), the correction interpolation induces two different schemes: one associated with even-number nodes and the other with odd-number ones. Thus, we will study the scheme associated with a couple of nodes $(N_{2p}, N_{2p+1})^t$ for $p = 0, ..., (n_h - 1)/2$. We will follow the two-grid scheme algorithm as it is described in Section 2, inserting a couple of harmonic data,

$$u_{h_{2p}}^n = \hat{u}_h^n e^{i2p\theta_h}$$
$$v_{h_{2p+1}}^n = \hat{v}_h^n e^{i(2p+1)\theta_h}$$

for $p = 0, ..., (n_h - 1)/2$, with $\hat{u}_h^0 = \hat{v}_h^0$.

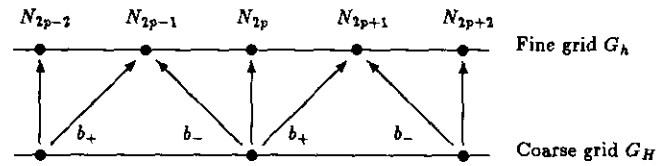

FIG. 3. Operator $\mathbf{I}_{H \mapsto h}$ in 1D.

The objective of this analysis is to determine the (2×2) matrix **MG** such that

$$\begin{pmatrix}\hat{u}_h^{n+1}\\ \hat{v}_h^{n+1}\end{pmatrix}=\mathbf{MG}(a_+,a_-,b_+,b_-,\alpha_H,\sigma_H,\alpha_h,\sigma_h,\theta_h)\times\begin{pmatrix}\hat{u}_h^{n}\\ \hat{v}_h^{n}\end{pmatrix}.$$

Let us introduce the following notations:

• Writing $z_h(\theta_h)$ (resulting from relations (12) and (13) (with $g=h$) for first and higher order space accuracy respectively), under the form $z_h(\theta_h)=\sum_h \eta_q e^{iq\theta_h}$ leads to the definition of both coefficients,

$$z_{e_h}(\theta_h)=\sum_p \eta_{2p}e^{i(2p)\theta_h}$$

$$z_{o_h}(\theta_h)=\sum_p \eta_{2p+1}e^{i(2p+1)\theta_h},$$

where $z_{e_h}(\theta_h)+z_{o_h}(\theta_h)=z_h(\theta_h)$. Then we denote by $\mathbf{Z}_h(\alpha_h,\sigma_h,\theta_h)$ the (2×2) matrix with the structure:

$$\mathbf{Z}_h(\theta_h)=\begin{pmatrix}z_{e_h}(\theta_h) & z_{o_h}(\theta_h)\\ z_{o_h}(\theta_h) & z_{e_h}(\theta_h)\end{pmatrix}$$

• Writing $g_h(\alpha_h,\sigma_h,\theta_h)$ (resulting from relation (14) with $g=h$), under the general form $g_h(\alpha_h,\sigma_h,\theta_h)=\sum_q \xi_q(\alpha_h,\sigma_h)e^{iq\theta_h}$ leads to the definition of both following coefficients:

$$g_{e_h}(\alpha_h,\sigma_h,\theta_h)=\sum_p \xi_{2p}(\alpha_h,\sigma_h)\,e^{i(2p)\theta_h}$$

$$g_{o_h}(\alpha_h,\sigma_h,\theta_h)=\sum_p \xi_{2p+1}(\alpha_h,\sigma_h)\,e^{i(2p+1)\theta_h}$$

where $g_{e_h}(\alpha_h,\sigma_h,\theta_h)+g_{o_h}(\alpha_h,\sigma_h,\theta_h)=g_h(\alpha_h,\sigma_h,\theta_h)$. Then we denote by $\mathbf{G}_h(\alpha_h,\sigma_h,\theta_h)$ the (2×2) matrix with the structure:

$$\mathbf{G}_h(\alpha_h,\sigma_h,\theta_h)=\begin{pmatrix}g_{e_h}(\alpha_h,\sigma_h,\theta_h) & g_{o_h}(\alpha_h,\sigma_h,\theta_h)\\ g_{o_h}(\alpha_h,\sigma_h,\theta_h) & g_{e_h}(\alpha_h,\sigma_h,\theta_h)\end{pmatrix}$$

Using the notations introduced in Section 2, we can write

$$\begin{aligned}\begin{pmatrix}\hat{u}_h^{n+1}\\ \hat{v}_h^{n+1}\end{pmatrix}&=[\mathbf{G}_h(\alpha_h,\sigma_h,\theta_h)]^{\nu_h^2}\begin{pmatrix}\hat{u}_h^{c}\\ \hat{v}_h^{c}\end{pmatrix}\\&=[\mathbf{G}_h(\alpha_h,\sigma_h,\theta_h)]^{\nu_h^2}\left[\begin{pmatrix}\hat{u}_h^{a}\\ \hat{v}_h^{a}\end{pmatrix}+\boldsymbol{I}_{H\mapsto h}(\hat{C}_H)\right]\\&=[\mathbf{G}_h(\alpha_h,\sigma_h,\theta_h)]^{\nu_h^2}\\&\quad\times\left[\begin{pmatrix}\hat{u}_h^{a}\\ \hat{v}_h^{a}\end{pmatrix}+\begin{pmatrix}1\\ b_+e^{-i\theta_h}+b_-e^{i\theta_h}\end{pmatrix}\hat{C}_H\right],\end{aligned}\tag{18}$$

where the approximate solution $(\hat{u}_h^a,\hat{v}_h^a)$ is given by

$$\begin{pmatrix}\hat{u}_h^{a}\\ \hat{v}_h^{a}\end{pmatrix}=[\mathbf{G}_h(\alpha_h,\sigma_h,\theta_h)]^{\nu_h^1}\begin{pmatrix}\hat{u}_h^{n}\\ \hat{v}_h^{n}\end{pmatrix}\tag{19}$$

and the coarse grid correction $\hat{C}_H$ can be expressed as

$$\begin{aligned}\hat{C}_H&=-\frac{1-[g_H(\alpha_H,\sigma_H,\theta_H)]^{\nu_H^1}}{|c|\,z_H(\theta_H)}\\&\quad\times\bar{\mathbf{I}}_{h\mapsto H}\left[|c|\,\mathbf{Z}_h(\theta_h)\begin{pmatrix}\hat{u}_h^{a}\\ \hat{v}_h^{a}\end{pmatrix}\right]\\&=-\frac{1-[g_H(\alpha_H,\sigma_H,\theta_H)]^{\nu_H^1}}{z_H(\theta_H)}\\&\quad\times(1,a_+e^{-i\theta_h}+a_-e^{i\theta_h})\,\boldsymbol{Z}_h(\theta_h)\begin{pmatrix}\hat{u}_h^{a}\\ \hat{v}_h^{a}\end{pmatrix},\end{aligned}\tag{20}$$

where $\theta_H=2\theta_h$.

Remark 4. In the previous expressions, a division by zero can occur only if $\kappa=1$ (corresponding to the centered scheme).

Remark 5. For an ideal two-grid cycle (i.e., ν_H^1 so that convergence on coarse grid can be supposed complete), we obtain

$$\hat{C}_H=\begin{cases}0, & \text{for } \theta_H=0 \text{ or } \theta_H=2\pi\\ -\dfrac{1}{|c|\,z_H(\theta_H)}\bar{\mathbf{I}}_{h\mapsto H}(\hat{R}_h^a), & \text{for } \theta_H\in\,]0,2\pi[.\end{cases}$$

Using relations (18)–(20), the amplification matrix is then given by

$$\begin{aligned}&\mathbf{MG}(a_+,a_-,b_+,b_-,\alpha_H,\sigma_H,\alpha_h,\sigma_h,\theta_h)\\&\quad=[\mathbf{G}_h(\alpha_h,\sigma_h,\theta_h)]^{\nu_h^2}\times\left[\mathbf{I}_2-\frac{1-[g_H(\alpha_H,\sigma_H,\theta_H)]^{\nu_H^1}}{z_H(\theta_H)}\right.\\&\qquad\left.\times\begin{pmatrix}1\\ b_+e^{-i\theta_h}+b_-e^{i\theta_h}\end{pmatrix}(1,a_+e^{-i\theta_h}+a_-e^{i\theta_h})\,\mathbf{Z}_h\right]\\&\qquad\times[\mathbf{G}_h(\alpha_h,\sigma_h,\theta_h)]^{\nu_h^2},\end{aligned}$$

where $\mathbf{I}_2$ is the (2×2) identity matrix.

The amplification factor of the two-grid method is then defined, for any wave number $\theta_h\in[0,\pi]$, as the maximum between the two eigenvalue modules of the matrix **MG**.

3.3. *Characteristic Multigrid Method in* 1D

We should specify the values of the coefficients a_+, a_-, b_+, b_-, defining the interpolation operators $\bar{\mathbf{I}}_{h\mapsto H}$ and $\mathbf{I}_{H\mapsto h}$, respectively. These coefficients are taken as equal to

$\frac{1}{2}$ in the standard multigrid method (that we call geometric multigrid or GM method) since fine grid nodes are middle points of two coarse grid nodes. This definition is in fact more restrictive than the necessary and sufficient conditions $a_+ + a_- = 1$, $b_+ + b_- = 1$. We introduce the characteristic multigrid (CM) method based on the new coefficients:

$$\text{or/and} \quad \begin{aligned} a_+ &= \frac{c^+}{c}, \quad a_- = \frac{c^-}{c} \\ b_+ &= \frac{c^+}{c}, \quad b_- = \frac{c^-}{c}. \end{aligned} \tag{21}$$

The definition (21) corresponds to an upwinding in the characteristic direction.

Remark 6. Both multigrid schemes obtained with one characteristic operator and one geometric operator are equivalent for the 1D linear case.

We will denote the different combinations and their respective amplification factors by:

$$\mathbf{GM} \to \mathscr{A}\mathscr{F}_{\mathrm{GM}}(\alpha_h, \sigma_h, \theta_h)$$

geometric residual restriction–geometric correction interpolation;

$$\mathbf{CM} \to \mathscr{A}\mathscr{F}_{\mathrm{CM}}(\alpha_h, \sigma_h, \theta_h)$$

characteristic residual restriction–geometric correction interpolation or geometric residual restriction–characteristic correction interpolation;

$$\mathbf{CCM} \to \mathscr{A}\mathscr{F}_{\mathrm{CCM}}(\alpha_h, \sigma_h, \theta_h)$$

characteristic residual restriction–characteristic correction interpolation.

As an extension to the case of a system of nonlinear hyperbolic equation in two dimensions can be achieved and will be proposed in Section 4. Some numerical tests have been performed to determine which one is the best adapted to this extension.

3.4. *Numerical Tests in 1D*

We consider an ideal two-grid cycle, consequently, multigrid amplification factors do not depend on coarse grid multi-stage parameters ($(\alpha_{H_k})_{k=1,\ldots,4}$ and σ_H) any longer and the space approximation is always supposed to be second-order accurate with $\kappa = 0$.

At first, we recall two four-stage schemes which were optimized by a single-grid analysis with respect to two different criteria. The first one, proposed by M. H. Lallemand [13], fulfills the three following conditions:

1. The highest frequency ($\theta_h = \pi$) is completely damped.

2. The value $\mathscr{A}\mathscr{F}_h(\alpha_h, \sigma_h, \theta_h = \pi)$ remains "small" in the (Courant number) interval $[\sigma_{h_1}, \sigma_{h_2}]$, where σ_{h_1} is as "large" as possible

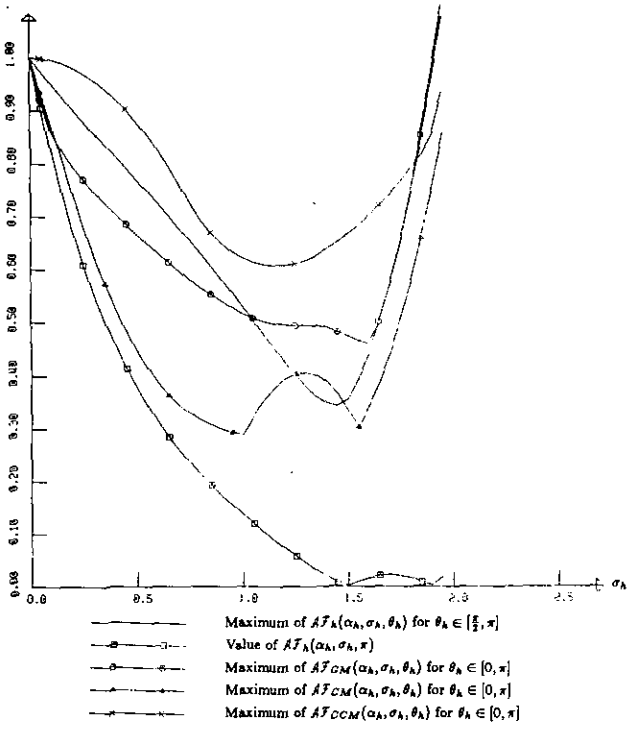

FIG. 4. Amplification factors as a function of Courant number with $\alpha_{h_1} = 0.11$, $\alpha_{h_2} = 0.2766$, $\alpha_{h_3} = 0.5$, $\alpha_{h_4} = 1$. Second-order space approximation, $\kappa = 0$.

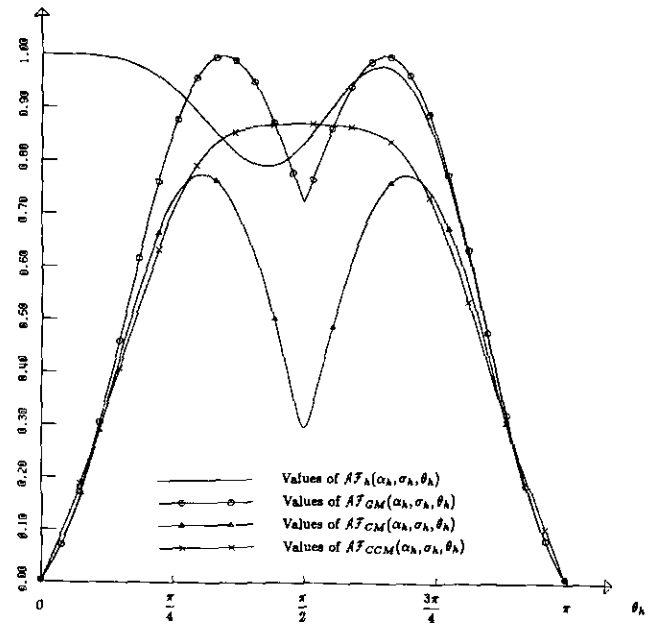

FIG. 5. Amplification factors as a function of the wave number with $\sigma_h = 1.91$, $\alpha_{h_1} = 0.11$, $\alpha_{h_2} = 0.2766$, $\alpha_{h_3} = 0.5$, $\alpha_{h_4} = 1$. Second-order space approximation, $\kappa = 0$.

3. The scheme is second-order accurate in time (i.e., $\alpha_{h_3} = 0.5$) and leads to the coefficients:

$$\alpha_{h_1} = 0.11, \quad \alpha_{h_2} = 0.2766, \quad \alpha_{h_3} = 0.5, \quad \alpha_{h_4} = 1, \quad \sigma_h = 1.91. \tag{22}$$

The second one is the optimal four-stage scheme regarding the damping of the high frequencies ($\pi/2 \leqslant \theta_h \leqslant \pi$) built with the method proposed by van Leer *et al.* [18] and gives

$$\alpha_{h_1} = 0.14, \quad \alpha_{h_2} = 0.2939, \quad \alpha_{h_3} = 0.5252, \quad \alpha_{h_4} = 1, \quad \sigma_h = 1.4. \tag{32}$$

Later, we have optimized the four-stage scheme coefficients, using the aforementioned multigrid analysis, with respect to the criterion: find α_{h_1}, α_{h_2}, α_{h_3}, and σ_h such that $\max_{\theta_h \in [0,\pi]} \mathscr{AF}_{\mathrm{MG}}(\alpha_h, \sigma_h, \theta_h)$ is minimal.

Corresponding to each multigrid method described above, we have found the coefficients:

$$\textbf{GM}, \quad \alpha_{h_1} = 0.1602, \ \alpha_{h_2} = 0.3297, \ \alpha_{h_3} = 0.5748, \ \alpha_{h_4} = 1, \ \sigma_h = 1.32 \tag{24}$$

$$\textbf{CM}, \quad \alpha_{h_1} = 0.1427, \ \alpha_{h_2} = 0.3026, \ \alpha_{h_3} = 0.5311, \ \alpha_{h_4} = 1, \ \sigma_h = 1.39 \tag{25}$$

$$\textbf{CCM}, \quad \alpha_{h_1} = 0.1372, \ \alpha_{h_2} = 0.2617, \ \alpha_{h_3} = 0.5245, \ \alpha_{h_4} = 1, \ \sigma_h = 1.4 \tag{26}$$

which are quite close to those of van Leer *et al.* (23).

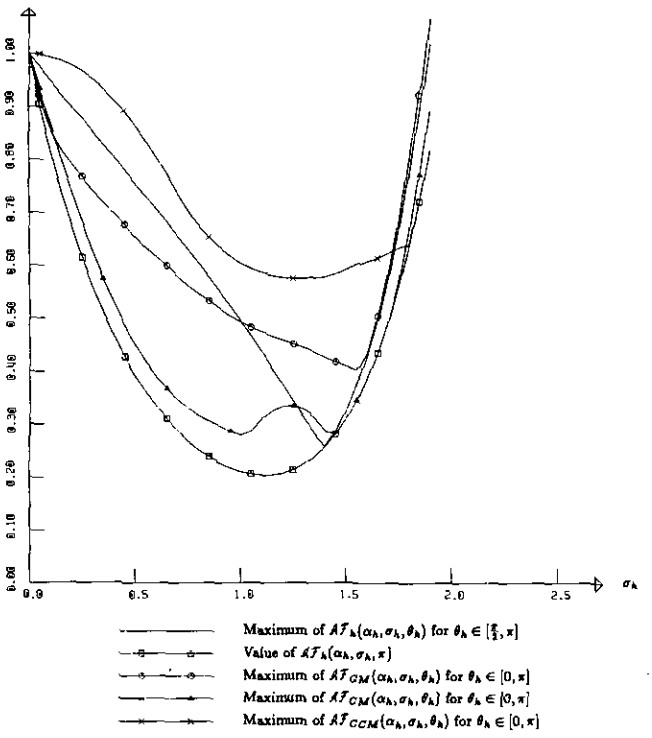

FIG. 6. Amplification factors as a function of Courant number with $\alpha_{h_1} = 0.14$, $\alpha_{h_2} = 0.2939$, $\alpha_{h_3} = 0.5252$, $\alpha_{h_4} = 1$. Second-order space approximation, $\kappa = 0$.

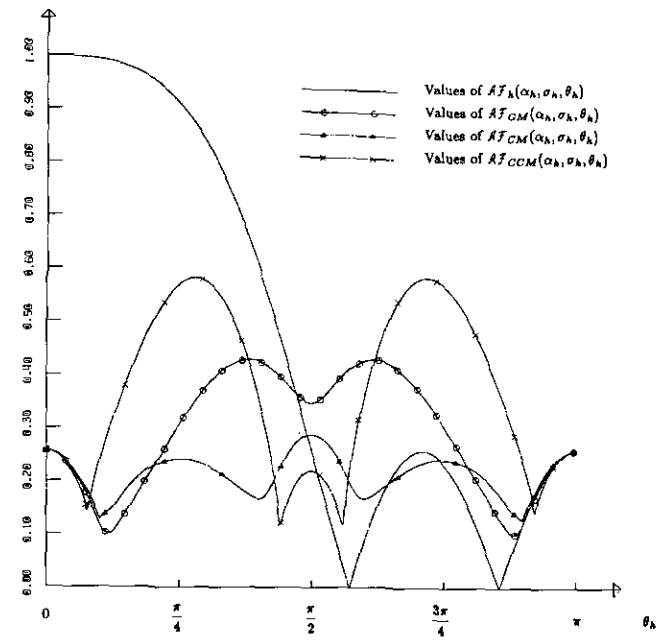

FIG. 7. Amplification factors as a function of the wave number with $\sigma_h = 1.4$, $\alpha_{h_1} = 0.14$, $\alpha_{h_2} = 0.2939$, $\alpha_{h_3} = 0.5252$, $\alpha_{h_4} = 1$. Second-order space approximation, $\kappa = 0$.

We compare the behavior of either the single-grid and the multigrid amplification factors considered as a function of the wave number with the optimal Courant number value, or the derived quantities $\mathscr{AF}_h(\alpha_h, \sigma_h, \pi)$ and $\max \mathscr{AF}_h(\alpha_h, \sigma_h, \theta_h)$ for $\theta_h \in [\pi/2, \pi]$ for the single-grid method and $\max \mathscr{AF}_{\mathrm{MG}}(\alpha_h, \sigma_h, \theta_h)$ for $\theta_h \in [0, \pi]$ for the multigrid methods (where "MG" designates GM, CM, or, CCM as a function of the Courant number.

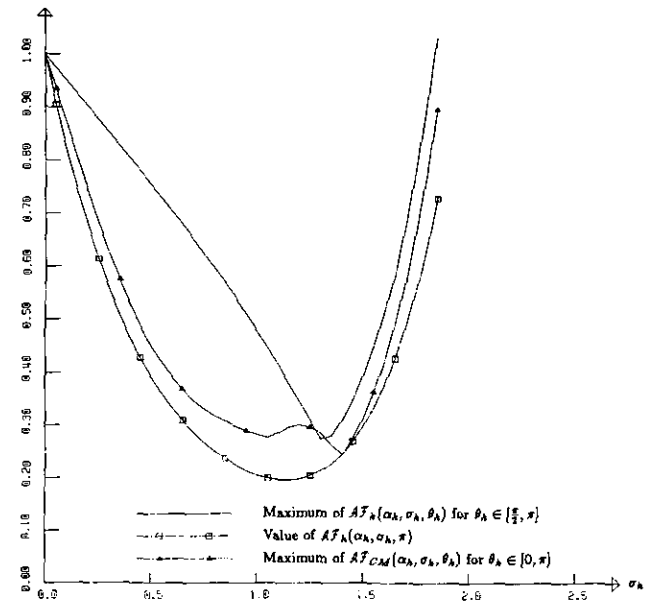

FIG. 8. Amplification factors as a function of Courant number with $\alpha_{h_1} = 0.1427$, $\alpha_{h_2} = 0.3026$, $\alpha_{h_3} = 0.5311$, $\alpha_{h_4} = 1$. Second-order space approximation, $\kappa = 0$.

TABLE I

Maximal Values of Amplification Factors for the Optimum Courant Number Value

	$\mathcal{AF}_h$ $\theta_h=\pi$	$\max_{\theta_h\in[\pi/2,\pi]} \mathcal{AF}_h$	$\max_{\theta_h\in[0,\pi]} \mathcal{AF}_{GM}$	$\max_{\theta_h\in[0,\pi]} \mathcal{AF}_{CM}$	$\max_{\theta_h\in[0,\pi]} \mathcal{AF}_{CCM}$
$\alpha_h, \sigma_h=(22)$	0.000	0.978	0.998	0.774	0.869
$\alpha_h, \sigma_h=(23)$	0.257	0.257	0.428	0.287	0.581
$\alpha_h, \sigma_h=(24)$	0.353	0.354	0.358	—	—
$\alpha_h, \sigma_h=(25)$	0.241	0.304	—	0.242	—
$\alpha_h, \sigma_h=(26)$	0.456	0.456	—	—	0.456

The obtained result is summarized in Table I. We consider the single-grid results (the first two lines of Table I) as a reference and we note an improvement when using one characteristic and one geometric operators (fourth line of the Table I).

The resulting curves are presented in Figs. 4, 6, 8 with respect to the Courant number and in Fig. 5, 7, 9 with respect to the wave number, for the optimal Courant number value.

4. ADAPTATION TO THE TWO-DIMENSIONAL NON-LINEAR CASE

In this section, we suggest a way to extend the previous 1D scalar linear analysis to a non-linear system in two dimensions: the Euler equations.

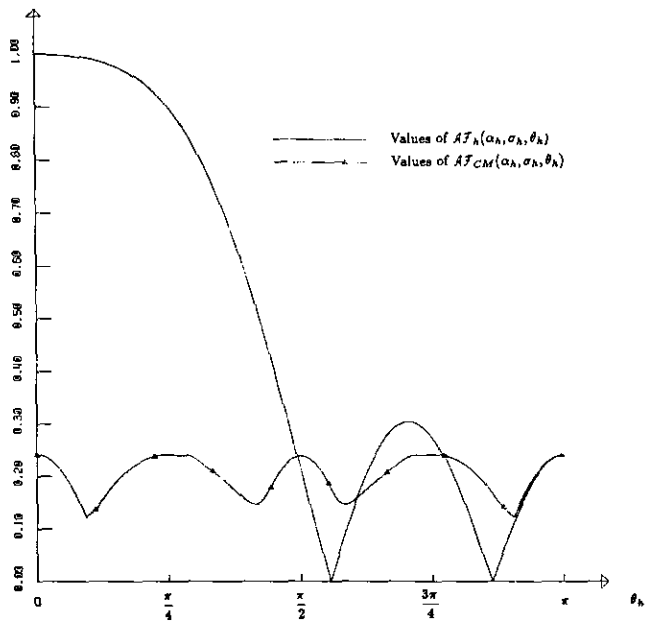

FIG. 9. Amplification factors as a function of the wave number with $\sigma_h=1.39$, $\alpha_{h_1}=0.1427$, $\alpha_{h_2}=0.3026$, $\alpha_{h_3}=0.5311$, $\alpha_{h_4}=1$. Second-order space approximation, $\kappa=0$.

4.1. *Mathematical Modeling*

We will present in this section the main features of a high order approximation of the Euler equations, relying on an upwind formulation on an unstructured mesh in conjunction with total variation diminushing (TVD) properties.

Let $\mathcal{T}_g$ be a triangulation of the computational domain Ω with boundary Γ. We can write the Euler system in a conservative form such as

$$\frac{\partial \mathbf{W}}{\partial t}+\nabla\cdot\mathbf{F}(\mathbf{W})=\mathbf{S},$$

where $\mathbf{S}$ is a source term that is supposed to be equal to zero on the fine grid.

The complete formulation can be found in [7] and uses a Green formula,

$$\text{Find } \mathbf{W}_g\in(\mathcal{V}_g)^m \quad \text{such that} \quad \forall N_{g_i}\in\mathcal{T}_g,$$

$$\int_{C_{g_i}}\frac{\partial \mathbf{W}_g}{\partial t}\,d\mathbf{x}+\int_{\partial C_{g_i}}\mathbf{F}(\mathbf{W}_g)\cdot\mathbf{n}_{g_i}\,d\sigma$$

$$+\int_{\partial C_{g_i}\cap\Gamma}\mathbf{F}(\mathbf{W}_g)\cdot\mathbf{n}_\Gamma\,d\sigma=\int_{C_{g_i}}\mathbf{S}_g\,d\mathbf{x} \qquad (27)$$

$$\mathbf{R}_{g_i}\overset{\text{def}}{=}-\int_{C_{g_i}}\mathbf{S}_g\,d\mathbf{x}+\int_{\partial C_{g_i}}\mathbf{F}(\mathbf{W}_g)\cdot\mathbf{n}_{g_i}\,d\sigma$$

$$+\int_{\partial C_{g_i}\cap\Gamma}\mathbf{F}(\mathbf{W}_g)\cdot\mathbf{n}_\Gamma\,d\sigma,$$

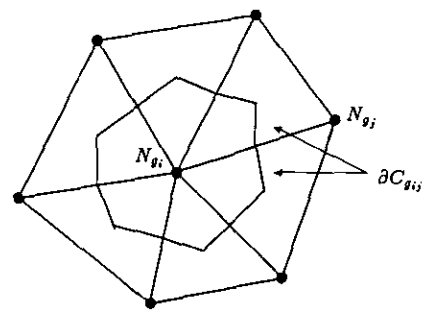

FIG. 10. Cell C_{g_i} of the dual mesh.

where $\mathscr{V}_g = \{W_g \in C^0(\Omega);\ W_g$ is linear on each triangle$\}$ and $\mathbf{R}_g$ denotes the residual. The cell C_{g_i} is defined for each vertex $N_{g_i} \in \mathscr{T}_g$, as the union of the subtriangles which have N_{g_i} as vertex and result from the subdivision of each triangle of $\mathscr{T}_g$ by means of the median planes as shown in Fig. 10. The vectors $\mathbf{n}_{g_i}$ and $\mathbf{n}_\Gamma$ designate outward normal vectors of the cell C_{g_i} and the domain boundary Γ, respectively.

The scheme will be completely defined if we now specify which approximation is used to compute the left-hand-side integral in (27). In order to do this, the boundary ∂C_{g_i} of the cell C_{g_i} is split into panels $\partial C_{g_{ij}}$, joining the segment $[N_{g_i}, N_{g_j}]$ to the centroids of the triangle having N_{g_i} and N_{g_j} as common vertices.

Let us give the notations:

$$\mathbf{F}_{ij}(\mathbf{W}_g) = \mathbf{F}(\mathbf{W}_g) \cdot \int_{\partial C_{g_{ij}}} \mathbf{n}_{g_i}\, d\sigma;$$

$$\mathbf{A}_{ij}(\mathbf{W}_g) = \frac{d}{d\mathbf{W}} \mathbf{F}(\mathbf{W}_g) \cdot \int_{\partial C_{g_{ij}}} \mathbf{n}_{g_i}\, d\sigma$$

$$\mathbf{P}_{ij}(\mathbf{W}_g) \qquad \text{such that}$$

$$\mathbf{P}_{ij}^{-1}(\mathbf{W}_g)\, \mathbf{A}_{ij}(\mathbf{W}_g)\, \mathbf{P}_{ij}(\mathbf{W}_g) = \mathbf{\Lambda}_{ij}(\mathbf{W}_g) \text{ a diagonal matrix.}$$

An upwinding is introduced in the evaluation of the convection term through the numerical flux function $\mathbf{\Phi}$ of a first-order accurate upwind scheme by

$$\int_{\partial C_{g_{ij}}} \mathbf{F}(\mathbf{W}_g) \cdot \mathbf{n}_i\, d\sigma = \mathbf{H}_{ij}^{(1)} = \mathbf{\Phi}_{F_{ij}}(\mathbf{W}_{g_i}, \mathbf{W}_{g_j}),$$

where $\mathbf{W}_{g_i} = \mathbf{W}_g(N_{g_i})$ and $\mathbf{W}_{g_j} = \mathbf{W}_g(N_{g_j})$.

The numerical flux function used in this scheme is Osher's approximate Riemann solver [24] which has been chosen because of its robustness and its parameter-free implementation. The numerical integration carried out with the upwind scheme, as described previously, leads to an approximation which is only first-order accurate. A second-order accurate MUSCL-like [16] extension can be defined without changing the approximation space

$$\text{Find } \mathbf{W}_g \in (\mathscr{V}_g)^m \qquad \text{such that}$$

$$\int_{C_{g_i}} \frac{\partial \mathbf{W}_g}{\partial t}\, d\mathbf{x} + \sum_{j \in K(i)} \mathbf{H}_{ij}^{(2)} \tag{28}$$

$$\int_{\partial C_{g_i} \cap \Gamma} \mathbf{F}(\mathbf{W}_g) \cdot \mathbf{n}_\Gamma\, d\sigma = \int_{C_{g_i}} S_g\, d\mathbf{x},$$

where $K(i)$ is the set of neighbours of vertex N_{g_i}, and $\mathbf{H}_{ij}^{(2)} = \mathbf{\Phi}_{F_{ij}}(\mathbf{W}_{g_{ij}}, \mathbf{W}_{g_{ji}})$.

The arguments $\mathbf{W}_{g_{ij}}$ and $\mathbf{W}_{g_{ji}}$ are values at the interface $\partial C_{g_{ij}}$ which have been interpolated by using upwind gradients as described below.

We define the downstream and upstream triangles $T_{g_{ij}}$ and $T_{g_{ji}}$ for each segment $[N_{g_i}, N_{g_j}]$ as shown in Fig. 11. Let the centered gradient be $\nabla \mathbf{W}_{g_{ij}} = \nabla \mathbf{W}_g|_{T_{g_{ij}}^\beta}$, where $T_{g_{ij}}^\beta$ is one of the triangles having N_{g_i} and N_{g_j} as vertices.

A good procedure, in terms of accuracy, is to use limiters on characteristic variables. We compute these variables by the transformation taken at the segment's midpoint. If we denote by $\mathbf{\Pi}_{ij}$ the eigenvector matrix corresponding to $\mathbf{P}_{ij}$ $((\mathbf{W}_{g_i} + \mathbf{W}_{g_j})/2)$, then the values at the interface needed to compute the flux $\mathbf{H}_{ij}^{(2)}$ (which are just an extension of the 1D case (10)) are given by

$$\mathbf{W}_{g_{ij}} = \mathbf{W}_{g_i} + \mathbf{\Pi}_{ij} \mathbf{Lc}_{ij} \mathbf{\Pi}_{ij}^{-1} \times \left(\frac{1-\kappa}{4} \nabla \mathbf{W}_g|_{T_{g_{ij}}} + \frac{1+\kappa}{4} \nabla \mathbf{W}_{g_{ij}} \right) \cdot \overrightarrow{N_{g_i} N_{g_j}},$$

where $\mathbf{Lc}_{ij}$, $\mathbf{Lc}_{ji}$ are the diagonal limiting matrices introduced to reduce numerical oscillations of the solution and to provide some kind of monotonicity property. In all computations, we use the Van Albada limiter [1] associated with the Fromm scheme corresponding to $\kappa = 0$, combining monotonicity and second-order accuracy [28].

Finally, boundary integrals over Γ are computed in order to take into account the physical boundary conditions.

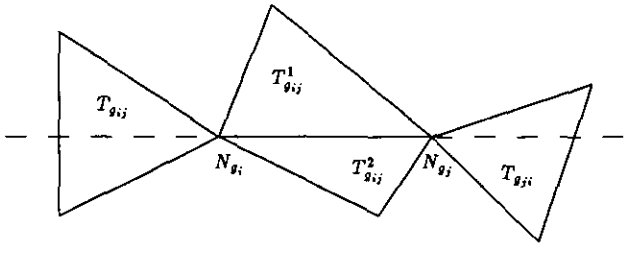

FIG. 11. Downstream and upstream triangles for the edge $[N_{g_i}, N_{g_j}]$.

5. CHARACTERISTIC MULTIGRID METHODS FOR NON-LINEAR PROBLEMS

The main feature of multigrid methods in a context of unstructured and unnested grids lies in the definition of transfer operators, which are generally only based on geometric principles. As it has been presented in Section 3, the characteristic multigrid technique takes into account the hyperbolicity of the problem into transfer operators too.

First, geometric operators will be described. Next, we will suggest a way that would modify the definition of the residual restriction operator $\bar{\mathbf{I}}_{h \to H}$.

5.1. *Geometric Transfer Operators in 2D*

The grids are supposed to be independent from each other, following [21]; we need information between two consecutive levels: for each node $N_h \in \mathcal{T}_h$ (resp. $N_H \in \mathcal{T}_H$), we should know which triangle $T_H(N_h) \in \mathcal{T}_H$ (resp. $T_h(N_H) \in \mathcal{T}_h$) contains N_h (resp. N_H) (Fig. 12).

We recall that the shape function $\mathcal{N}_{N_g}$ associated with a node $N_g \in \mathcal{T}_g$ is a linear function on each triangle of $\mathcal{T}_g$ and takes value 1 at node N_g and 0 at every other node:

- flow variable restriction operator $\mathbf{I}_{h \mapsto H}$,

$$\mathbf{W}_H(N_H) \overset{\text{def}}{=} \mathbf{I}_{h \mapsto H}(\mathbf{W}_h)(N_H) = \sum_{k=1}^{3} \mathcal{N}_{h_k}(N_H)\, \mathbf{W}_h(N_{h_k}),$$

where $N_H \in \mathcal{T}_H$; N_{h_1}, N_{h_2}, and N_{h_3} are the vertices of the triangle $T_h(N_H) \in \mathcal{T}_h$; and $\mathcal{N}_{h_k} \in \mathcal{V}_h$ is the shape function associated with the node N_{h_k}, for $k = 1, \ldots, 3$.

- correction prolongation operator $\mathbf{I}_{H \mapsto h}$,

$$(\mathbf{I}_{H \mapsto h}\, \mathbf{C}_H)(N_h) = \sum_{k=1}^{3} \mathcal{N}_{H_k}(N_h)\, \mathbf{C}_H(N_{H_k}),$$

where $N_h \in \mathcal{T}_h$; N_{H_1}, N_{H_2}, and N_{H_3} are the vertices of the triangle $T_H(N_h) \in \mathcal{T}_H$; and $\mathcal{N}_{H_k} \in \mathcal{V}_H$ is the shape function associated with the node N_{H_k}, for $k = 1, \ldots, 3$.

- residual restriction operator $\bar{\mathbf{I}}_{h \mapsto H}$. Let us define the set $\mathcal{C}_h(N_H) = \{N_h \in \mathcal{T}_h$ such that $T_H(N_h)$ has N_H as vertex$\}$. Then the restricted residual at node $N_H \in \mathcal{T}_H$ is collected from residuals at nodes $N_h \in \mathcal{C}_h(N_H)$,

$$(\bar{\mathbf{I}}_{h \mapsto H} \mathbf{R}_h)(N_H) = \sum_{N_h \in \mathcal{C}_h(N_H)} \mathcal{N}_{N_H}(N_h)\, \mathbf{R}_h(N_h), \tag{29}$$

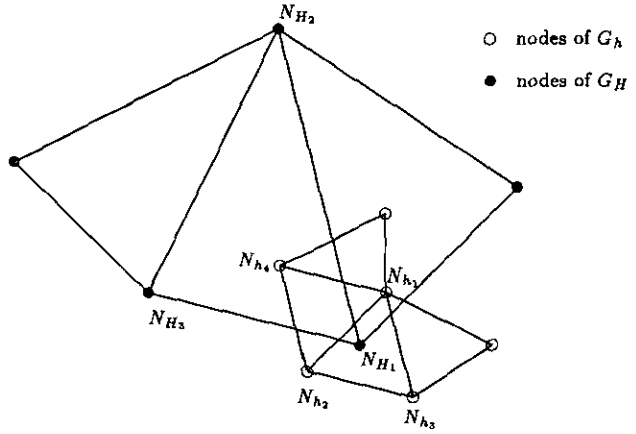

FIG. 12. Transfer operators in 2D: (a) fine grid residual at node N_{h_4} is linearly distributed to coarse grid restricted residuals at nodes N_{H_1}, N_{H_2}, N_{H_3}; (b) fine grid corrections at node N_{h_4} is a linear interpolation of coarse grid corrections at nodes N_{H_1}, N_{H_2} and N_{H_3}; (c) coarse grid flow variables at node N_{H_1} are a linear interpolation of fine grid flow variables at nodes N_{h_1}, N_{h_2} and N_{h_3}.

where $\mathcal{N}_{N_H} \in \mathcal{V}_H$ denotes the shape function associated with the node N_H.

5.2. *Characteristic Operator* $\bar{\mathbf{I}}_{h \mapsto H}$ *in 2D*

Let us introduce the following notations: Let $\mathbf{A}_\mathbf{d}(\mathbf{W}_h) = (d/d\mathbf{W})\ \mathbf{F}(\mathbf{W}_h) \cdot \mathbf{d}$ be the jacobian matrix, in the unitary direction $\mathbf{d}$ and $\mathbf{P}_\mathbf{d}(\mathbf{W}_h)$ the corresponding eigenvector matrix. We denote by $\mathbf{\Lambda}_\mathbf{d}(\mathbf{W}_h) = \text{diag}(\lambda^l_\mathbf{d}(\mathbf{W}_h))_{l=1,\ldots,4}$ the diagonal matrix

$$\mathbf{A}_\mathbf{d}(\mathbf{W}_h) = \mathbf{P}_\mathbf{d}(\mathbf{W}_h)\, \mathbf{\Lambda}_\mathbf{d}(\mathbf{W}_h)\, \mathbf{P}_\mathbf{d}^{-1}(\mathbf{W}_h)$$

with

$$\begin{aligned} \lambda^1_\mathbf{d}(\mathbf{W}_h) &= \mathbf{u} \cdot \mathbf{d} - c \\ \lambda^2_\mathbf{d}(\mathbf{W}_h) &= \lambda^3_\mathbf{d}(\mathbf{W}_h) = \mathbf{u} \cdot \mathbf{d} \\ \lambda^4_\mathbf{d}(\mathbf{W}_h) &= \mathbf{u} \cdot \mathbf{d} + c, \end{aligned} \tag{30}$$

where $\mathbf{u}$ is the speed vector and c is the local speed of sound.

The definition of $\bar{\mathbf{I}}_{h \mapsto H}$ given by (29) can be rewritten as

$$\begin{aligned} (\bar{\mathbf{I}}_{h \mapsto H}\, \mathbf{R}_h)(N_H) = \sum_{N_h \in \mathcal{C}_h(N_H)} & \mathcal{N}_{N_H}(N_h) \\ & \times [\mathbf{P}_{\mathbf{d}_H(N_h)}(\mathbf{W}_h)\, \mathbf{P}^{-1}_{\mathbf{d}_H(N_h)}(\mathbf{W}_h)] \\ & \times \mathbf{R}_h(N_h), \end{aligned} \tag{31}$$

where $\mathbf{d}_H(N_h)$ represents the unitary direction $\mathbf{N_h N_H} / \|\mathbf{N_h N_H}\|$ (see Fig. 13).

Let $\mathbf{Id}_4$ be the 4×4 identity matrix; we denote by

$$\mathbf{\Psi}_{N_H}(N_h) = \mathcal{N}_{N_H}(N_h)\, \mathbf{Id}_4 = \text{diag}(\psi^l_{N_H}(N_h))_{l=1,\ldots,4} \quad \text{for} \quad N_h \in \mathcal{C}_h(N_H)$$

then Eq. (31) reads:

$$\begin{aligned} (\bar{\mathbf{I}}_{h \mapsto H}\, \mathbf{R}_h)(N_H) = \sum_{N_h \in \mathcal{C}_h(N_H)} & \mathbf{P}_{\mathbf{d}_H(N_h)}(\mathbf{W}_h) \\ & \times \mathbf{\Psi}_{N_H}(N_h)\, \mathbf{P}^{-1}_{\mathbf{d}_H(N_h)}(\mathbf{W}_h)\, \mathbf{R}_h(N_h). \end{aligned} \tag{32}$$

It appears that the matrix $\mathbf{\Psi}_{N_H}(N_h)$, in (32), contains

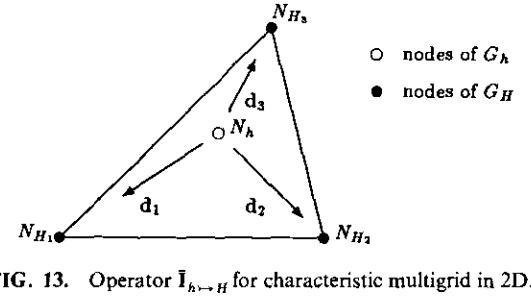

FIG. 13. Operator $\bar{\mathbf{I}}_{h \mapsto H}$ for characteristic multigrid in 2D.

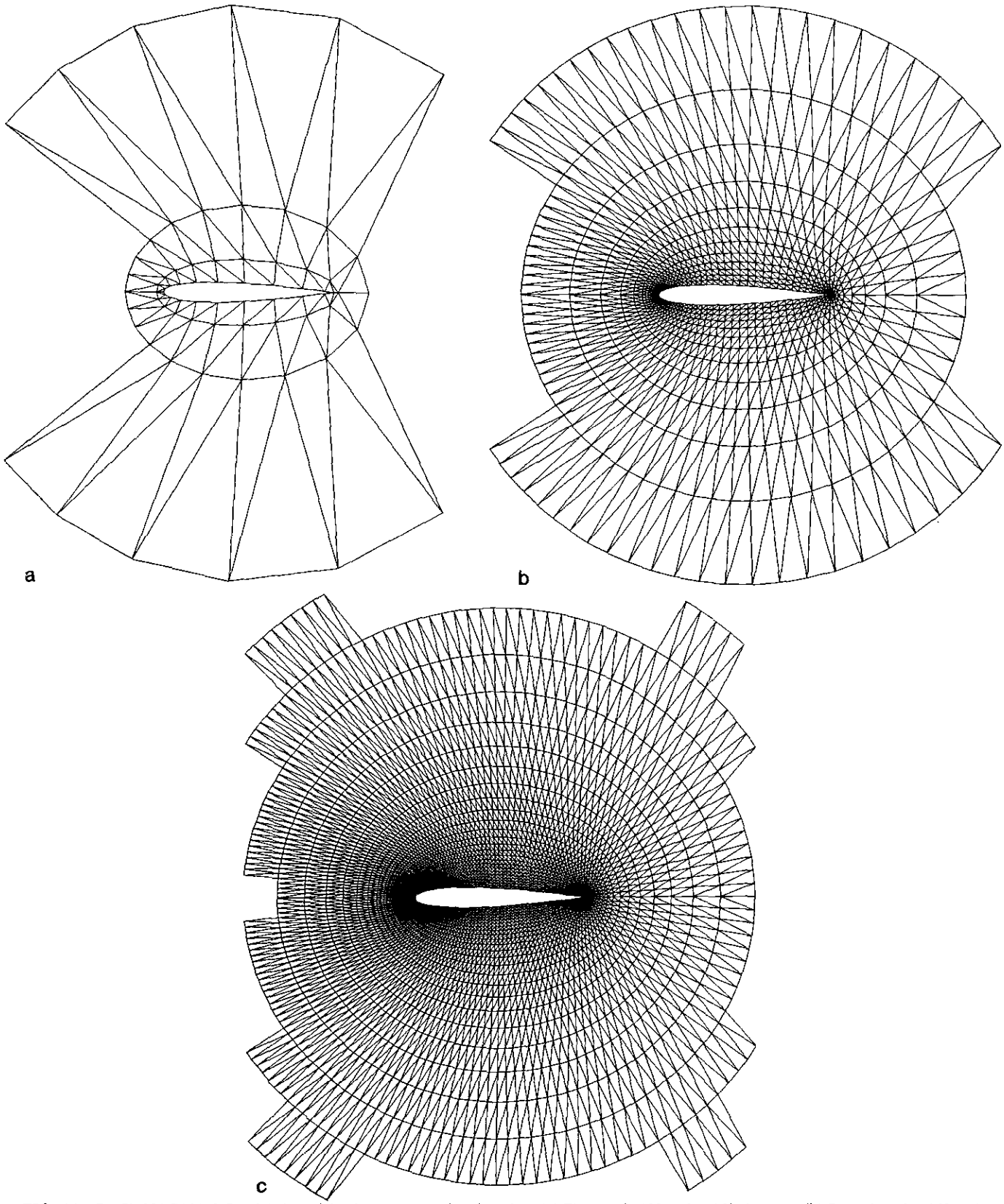

FIG. 14. Profile NACA0012. Partial view of the three computational meshes: (a) First mesh, 100 nodes, 160 elements; (b) Second mesh, 1360 nodes, 2560 elements; (c) Third mesh, 5280 nodes, 10,240 elements.

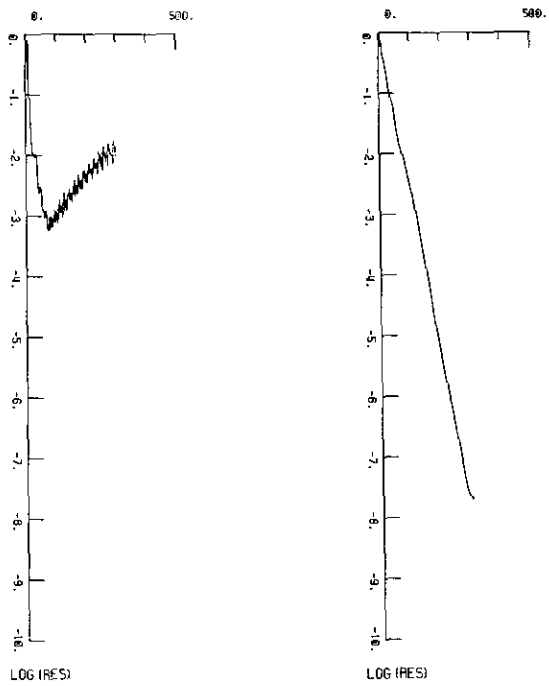

FIG. 15. Profile NACA0012, $M_\infty = 2$, $\alpha = 10°$. Convergence history versus the number of cycles: Curve 1, GM method; Curve 2, CM method.

the interpolation weights in the direction $\mathbf{d}_H(N_h)$ of the characteristic residual $\tilde{\mathbf{R}}_h(N_h) = \mathbf{P}^{-1}_{\mathbf{d}_H(N_h)}(\mathbf{W}_h)\ \mathbf{R}_h(N_h)$ (we recall that for the geometric operator, all the weights are equal).

The point of the characteristic multigrid is to weigh each characteristic component in an independent way, by using characteristic directions. We consider that the lth component of $\tilde{\mathbf{R}}_h(N_h)$ occurs if $\lambda^l_{\mathbf{d}_H(N_h)}(\mathbf{W}_h) > 0$. Consequently, an expression of the modified matrix $\mathbf{\Psi}_{N_H}(N_h)$ can be written as

$$\tilde{\psi}^l_{N_H}(N_h) = \begin{cases} \mathcal{N}_{N_H}(N_h) & \text{if } \lambda^l_{\mathbf{d}_H(N_h)}(\mathbf{W}_h) > 0 \\ 0 & \text{otherwise} \end{cases} \tag{33}$$

for $N_h \in \mathcal{C}_h(N_H)$ and $l = 1, ..., 4$.

However, conservation is lost with definition (33). As we want to preserve it, the corresponding equation, to ensure conservation per triangle,

$$\sum_{k=1}^{3} \tilde{\psi}^l_{N_{H_k}}(N_h) = 1 \qquad \text{for} \quad l = 1, ..., 4, \tag{34}$$

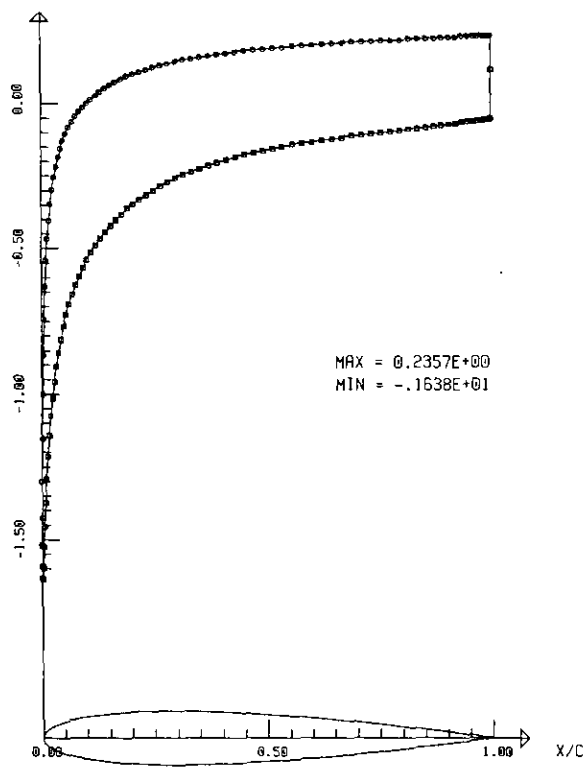

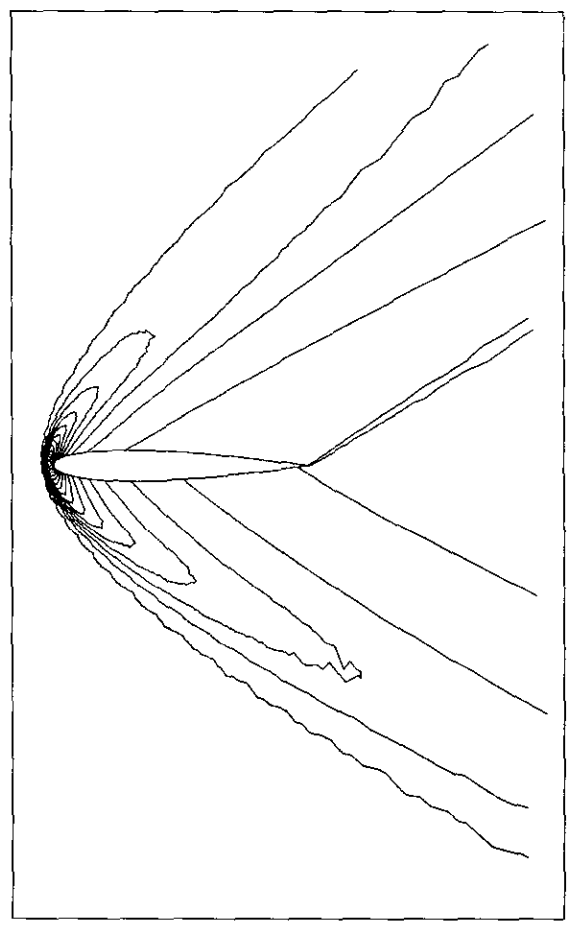

FIG. 16. Profile NACA0012, $M_\infty = 2$, $\alpha = 10°$. Iso-pressure coefficient lines and distribution on the body: ($A = 0.131$).

has to hold, where N_{H_1}, N_{H_2}, and N_{H_3} are the vertices of $T_H(N_h)$. If we denote by

$$\varphi^l(N_h) = \sum_{k=1}^{3} \psi^l_{N_{H_k}}(N_h) \quad \text{for} \quad l = 1, ..., 4 \tag{35}$$

then Eq. (34) can be fulfilled if the coefficients $(\tilde{\psi}^l_{N_H}(N_h))_{l=1,...,4}$ are rescaled by $\varphi^l(N_h)$ (35), provided that it should not be zero, for $l = 1, ..., 4$. Finally, the complete definition of operator $\bar{\mathbf{I}}_{h \mapsto H}$ in the characteristic multigrid context is given by

$$\psi^l_{N_H}(N_h) = \begin{cases} \dfrac{\tilde{\psi}^l_{N_H}(N_h)}{\varphi^l(N_h)} & \text{if } \lambda^l_{\mathbf{a}_H(N_h)}(\mathbf{W}_h) > 0 \\ & \text{and } \varphi^l(N_h) > 0 \\ \mathcal{N}_{N_H}(N_h) & \text{if } \varphi^l(N_h) = 0 \\ 0 & \text{if } \lambda^l_{\mathbf{a}_H(N_h)}(\mathbf{W}_h) \leqslant 0 \\ & \text{and } \varphi^l(N_h) > 0 \end{cases} \tag{36}$$

for $N_h \in \mathcal{C}_h(N_h)$ and $l = 1, ..., 4$, where $\varphi^l(N_h)$ results from (35) that uses (33).

6. NUMERICAL RESULTS

We will present a set of two computations, applying the methodology described below, to illustrate the capacities of the new multigrid solver. The first application of the multigrid technique is the computation of the flow around a NACA0012 airfoil at a Mach number of 2 and an angle of attack of 10°. The three computational meshes are displayed in Fig. 14, the coarsest mesh contains 100 nodes and 160 elements; the finest one contains 5280 nodes and 10,240 elements. The residual history (in $\mathbf{L}_2$-norm) versus the number of cycles of the GM and the CM methods using the corresponding optimized coefficients given by (24) and (25), respectively, are depicted in Fig. 15. The GM method is not

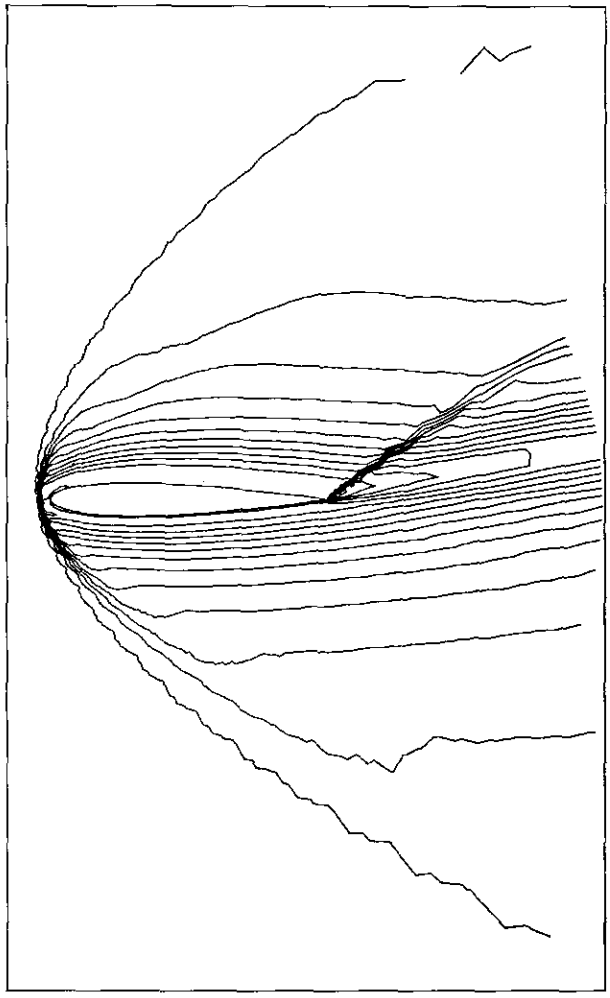

FIG. 17. Profile NACA0012, $M_\infty = 2$, $\alpha = 10°$. Iso-entropy lines: ($\Delta = 0.013$).

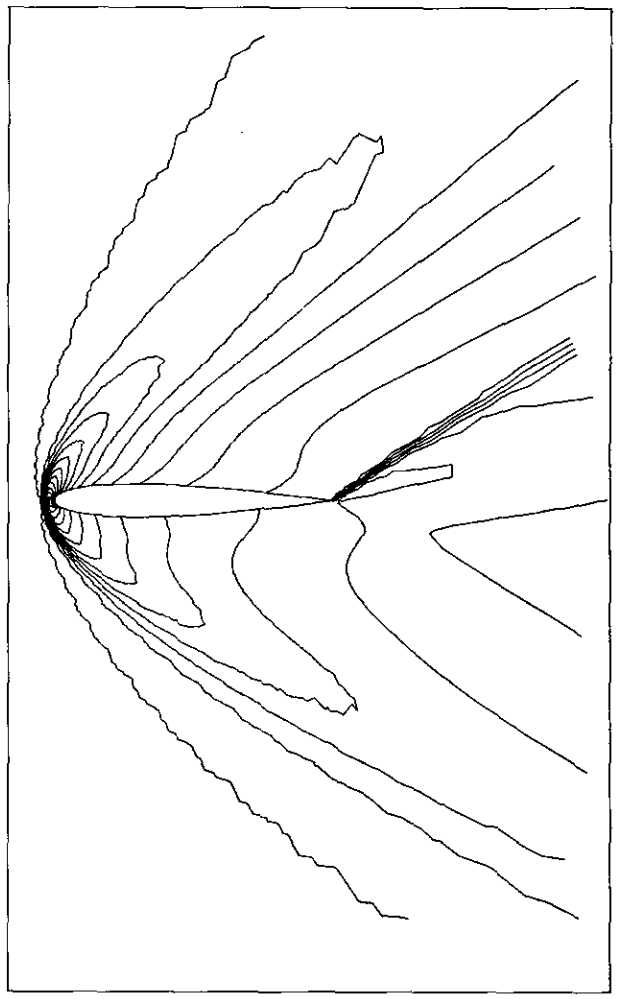

FIG. 18. Profile NACA0012, $M_\infty = 2$, $\alpha = 10°$. Iso-Mach number lines: ($\Delta = 0.13$).

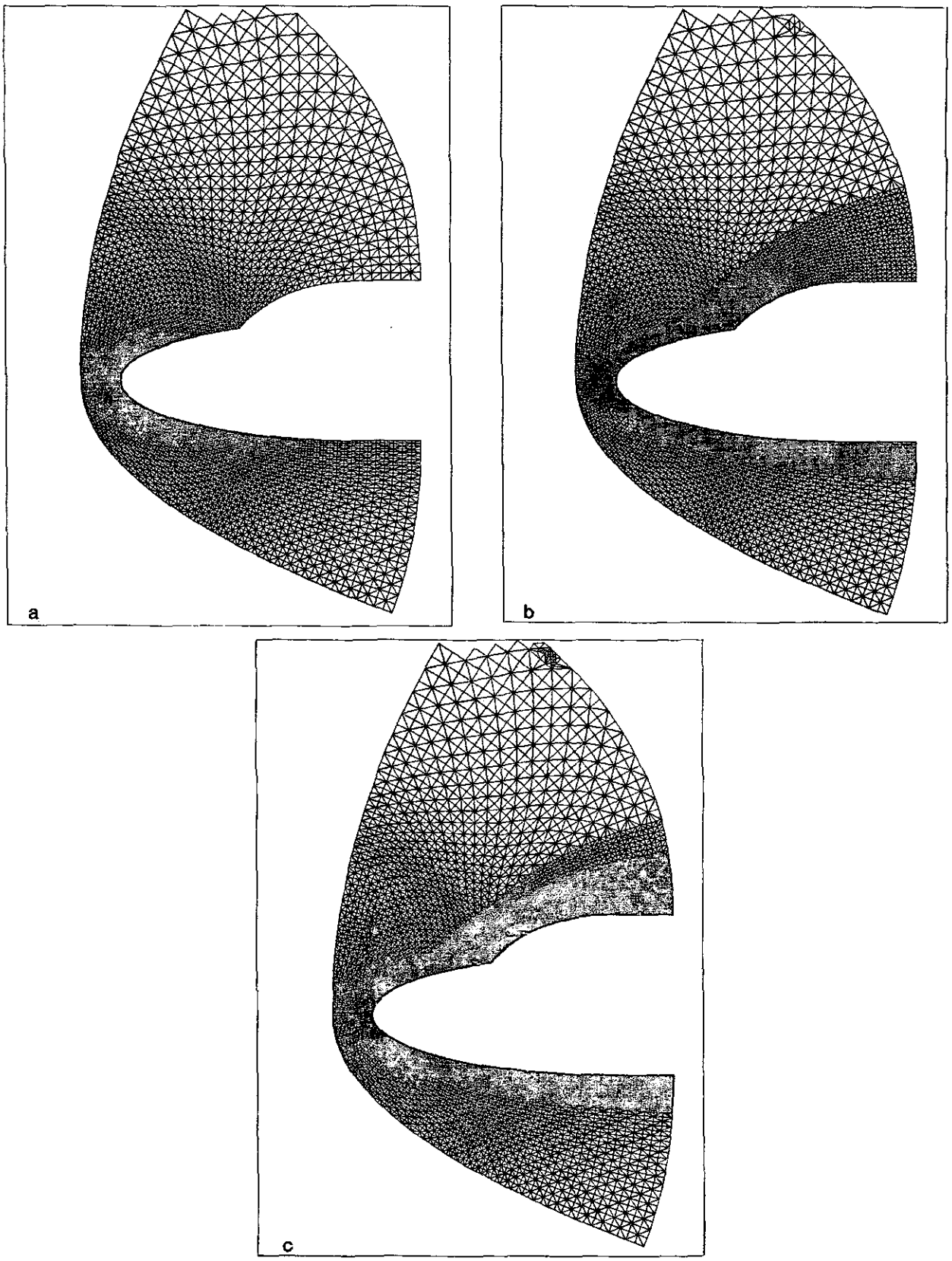

FIG. 19. Double ellipse. Partial view of the three computational meshes: (a) First mesh, 4257 nodes, 8192 elements; (b) Second mesh, 8441 nodes, 16,415 elements; (c) Third mesh, 14,827 nodes, 28,938 elements.

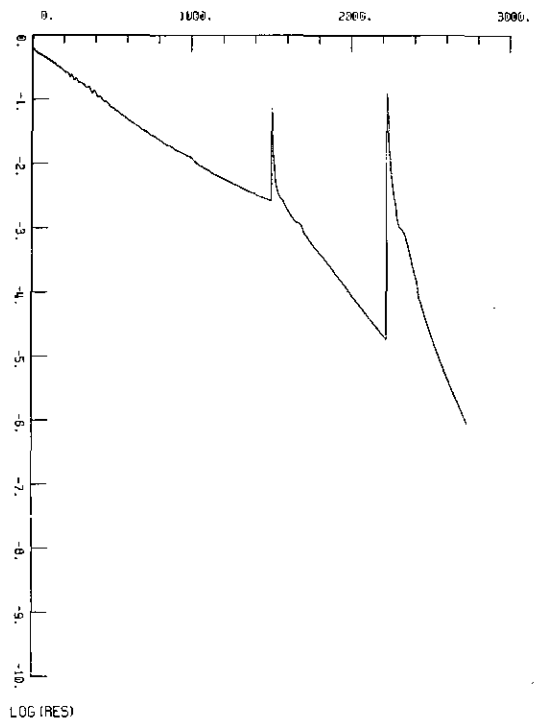

FIG. 20. Double ellipse, $M_\infty = 8.15$, $\alpha = 30°$. Convergence history versus the number of cycles.

able to give a result for this test case. The convergence of the CM method shows a decrease of residual by over eight orders of magnitude in about 300 cycles. This demonstrates the efficiency and reliability of this new multigrid solver. The iso-pressure coefficient lines and the corresponding distribution on the body (obtained on the finest grid) are plotted in Fig. 16. The iso-entropy lines displayed in Fig. 17 show the accuracy of the scheme and the iso-Mach number lines in Fig. 18 demonstrate the sharp capture of the shocks.

The next test case is the computation of the hypersonic flow around a double ellipse at a Mach number of 8.15 and an angle of attack of 30°, in order to check the robustness of the promising CM method. The sequence of three grids are presented in Fig. 19. The coarsest mesh contains 4257 nodes and 8192 elements; the finest one contains 14,827 nodes and 28,938 elements. The convergence history (in L_2-norm) versus the number of cycles is displayed in Fig. 20 when using the full-multigrid approach; the different convergence rates show a behavior better than expected (independent of the size of the finest mesh). The CM method has *successfully* computed this hypersonic flowfield in a small number of cycles. The iso-entropy lines and corresponding distribution (Fig. 21) prove the quality and accuracy of the unstructured grid solver. The iso-Mach number distribution in Fig. 22 indicates that the canopy shock is a detached one with a subsonic pocket.

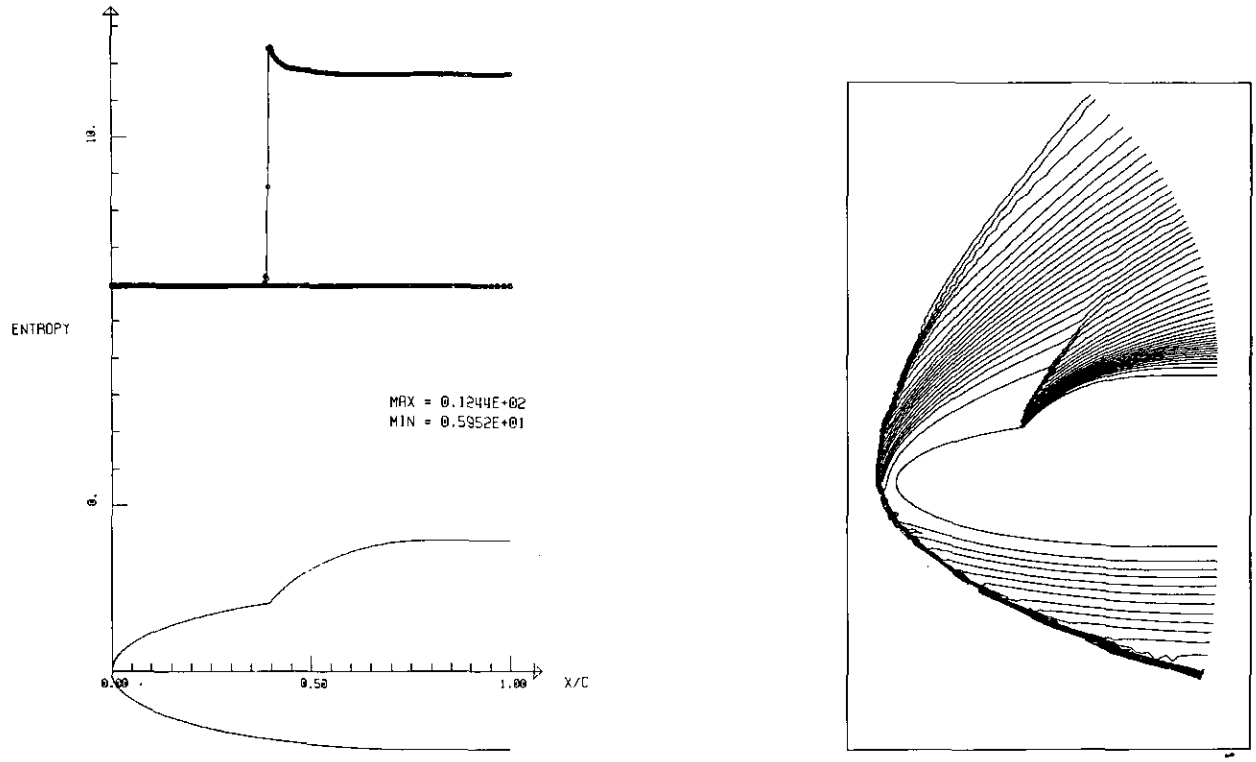

FIG. 21. Double ellipse, $M_\infty = 8.15$, $\alpha = 30°$. Iso-entropy lines and distribution on the body: ($\Delta = 0.250$).

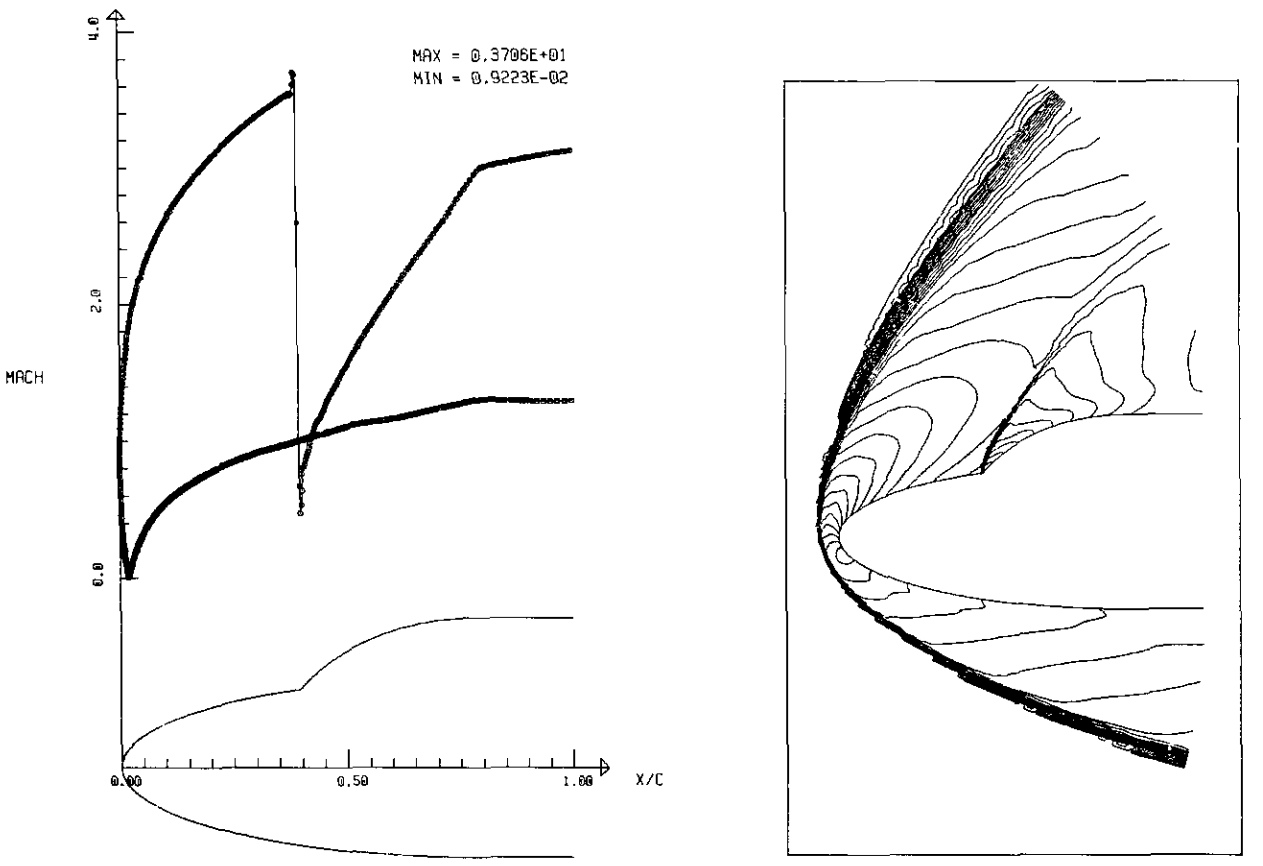

FIG. 22. Double ellipse, $M_\infty = 8.15$, $\alpha = 30°$. Iso-Mach number lines and distribution on the body: ($\Delta = 0.250$).

7. CONCLUSION

The one-dimensional Fourier analysis of the complete multigrid algorithm on the linear advection equation has clearly shown the advantages of the characteristic multigrid method. This result is confirmed by the numerical experiments performed with an unstructured multigrid method for two-dimensional Euler flow computations. The extension to 2D of the characteristic transfer operators has allowed the computation of severe problems such as hypersonic flows with strong detached shocks; this could not be possible with the classical approach.

ACKNOWLEDGMENTS

The authors thank A. Dervieux, M. H. Lallemand, and H. Stève for many helpful discussions and Renée Moes-Ravachol for proofreading.

REFERENCES

1. G. D. van Albada, B. van Leer, and W. W. Roberts, *Astron. Astrophys.* **108**, 76 (1982).
2. A. Brandt, Research report, Weizmann Institute of Sciences, Rehovot, Israel, 1981 (unpublished).
3. A. Brandt, G. M. D.-Studien Nr. 85, Gesellschaft für Mathematik und Datenverarbeitung, St. Augustin, May 1984 (unpublished).
4. V. Couailler, Thèse de l'Université Pierre et Marie Curie Paris VI, Septembre 1985 (unpublished).
5. V. Couailler and R. Peyret, *Rech. Aérospat.* (1986).
6. J. A. Désidéri, A. Goudjo, and V. Selmin. Rapport de Recherche INRIA 607, Février 1986 (unpublished).
7. L. Fézoui and B. Stoufflet, *J. Comput. Phys.* **84** (1), 174 (1989).
8. W. Hackbusch, *Computational Mathematics (4)* (Springer-Verlag, Berlin/Heidelberg/New York, 1985).
9. T. J. R. Hughes, L. P. Franca, I. Harari, M. Mallet, F. Shakib, and T. E. Spelse. AIAA Paper 87-0556, 1987 (unpublished).
10. A. Jameson, Report MAE 1743, October 1985 (unpublished).
11. A. Jameson, T. J. Baker, and N. P. Weatherill, AIAA Paper 86-0103, January 1986 (unpublished).
12. B. Koren and P. W. Hemker, Report NM-R 8922, CWI, Amsterdam, 1989 (unpublished).
13. M. H. Lallemand, Thèse de l'Université de Provence Aix-Marseille I, Mars 1988 (unpublished).
14. M. H. Lallemand and A. Dervieux, "A Multigrid Finite Element Method," Third Copper Montain Conference on Multigrid Methods, Colorado, April 1987.
15. M. P. Leclercq, J. Périaux, and B. Stoufflet, "Multigrid Methods with Unstructured Meshes," 7th International Conference on Finite Element Methods in Flow Problems, Hunstville (Alabama), April 3–7 1989.

16. B. van Leer, *J. Comput. Phys.* **23**, 263 (1977).
17. B. van Leer, in *Large-Scale Computations in Fluid Mechanics*, Lectures in Applied Mathematics, Vol. 22, 1985.
18. B. van Leer, C. H. Tai, and K. G. Powell, in *Large-Scale Computations in Fluid Mechanics*, Lectures in Applied Mathematics, Vol. 22, 1985.
19. R. Lohner, P. Parikh, and M. Salas, Report NASA Langley, VA, 1988.
20. J. F. Maitre and F. Musy, *Appl. Math. Comput.* **21**, 21 (1987).
21. D. Mavriplis and A. Jameson, AIAA Paper 87-0353, January 1987 (unpublished).
22. W. A. Mulder, *J. Comput. Phys.* **83** (2), 303 (1989).
23. R. H. Ni, *AIAA J.* **20** (11) (1982).
24. S. Osher and F. Salomon, *Math. Comput.* **38**, 339 (1988).
25. J. Peraire, J. Peiro, L. Formaggia, K. Morgan, and O. Zienkiewicz, AIAA Paper 88-0032, 1988 (unpublished).
26. E. Pérez, J. Périaux, J. P. Rosenblum, B. Stoufflet, A. Dervieux, and M. H. Lallemand, "Adaptative Full-Multigrid Finite Element Methods for Solving the Two-Dimensional Euler Equations," 10th International Conference on Numerical Methods in Fluid Dynamics, Beijing (China), June 1986.
27. R. Sanders and A. Weiser, Research Report UH/MD 56, March 1989 (unpublished).
28. S. P. Spekreijse, Thesis, CWI, Amsterdam, 1987 (unpublished).
29. H. Stève, Rapport de recherche INRIA 779, 1987 (unpublished).
30. B. Stoufflet, J. Périaux, L. Fézoui, and A. Dervieux, AIAA Paper 87-0560, 1987 (unpublished).
31. E. Turkel and B. van Leer, Report ICASE 84-27, June 1984 (unpublished).
32. R. Vichnevetsky and J. B. Bowles, *Fourier Analysis of Numerical Approximations of Hyperbolic Problems* (SIAM, Philadelphia, 1982).